Journal Pre-proof

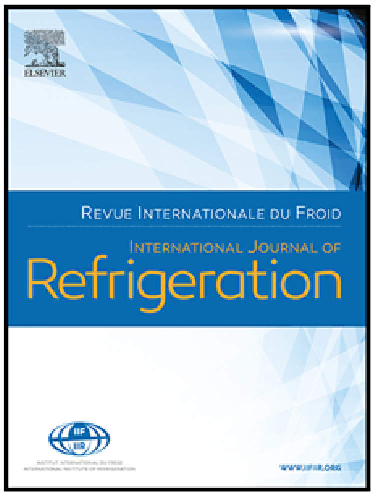

Investigation on the performance of fluted tube-in-tube gas cooler in transcritical CO_2 heat pump water heater

Zuliang Ye , Yikai Wang , Alireza Zendehboudi , Armin Hafner , Feng Cao

PII: S0140-7007(21)00505-3
DOI: https://doi.org/10.1016/j.ijrefrig.2021.12.011
Reference: JIJR 5379

To appear in: *International Journal of Refrigeration*

Received date: 20 October 2021
Revised date: 8 December 2021
Accepted date: 11 December 2021

Please cite this article as: Zuliang Ye , Yikai Wang , Alireza Zendehboudi , Armin Hafner , Feng Cao , Investigation on the performance of fluted tube-in-tube gas cooler in transcritical CO_2 heat pump water heater, *International Journal of Refrigeration* (2021), doi: https://doi.org/10.1016/j.ijrefrig.2021.12.011

Highlights:

- The model obtained CO_2 outlet temperature with an absolute mean error of 1.14 K.
- The heat transfer rate of fluted tube-in-tube gas cooler was generally higher.
- The improvement of maximum COP could be up to 29.41% by using the fluted tube.
- The COP improvement could be impaired to 6.30% at water inlet temperature of 40℃.

Investigation on the performance of fluted tube-in-tube gas cooler in transcritical CO_2 heat pump water heater

Zuliang Ye[a,b], Yikai Wang[a], Alireza Zendehboudi[b], Armin Hafner[b], Feng Cao[a,*]

[a] School of Energy and Power Engineering, Xi'an Jiaotong University, 28 Xianning West Road, Xi'an 710049, China

[b] Department of Energy and Process Engineering, Norwegian University of Science and Technology (NTNU), Kolbjørn Hejes v 1B, 7491 Trondheim, Norway

* Corresponding author, Email: fcao@mail.xjtu.edu.cn; Tel: 86-29-82663583;

Fax: 86-029-82663583

Abstract

The utilization of fluted inner tube in tube-in-tube heat exchangers is an effective way to improve the heat transfer performance. Based on the segmented model, the performance of a fluted tube-in-tube gas cooler (FTGC) in the transcritical CO_2 heat pump water heater was studied in this paper. The simulation model was validated and adopted to numerically investigate the effects of different parameters on the heat transfer performance of the gas cooler, which was compared to the smooth tube-in-tube gas cooler (STGC) with the same geometric parameters. The results showed that the FTGC had higher heat transfer capacity in most conditions. The heat transfer rate first increased and then decreased as the CO_2 inlet pressure increased. The temperature difference at the pinch point in the FTGC was lower than that in the STGC. In the FTGC, the pinch point position was mainly influenced by the CO_2 inlet pressure and water inlet and outlet temperatures. Regarding the system COP, the improvement of maximum COP could be up to 29.41% by using the FTGC compared to STGC when the water inlet temperature was 10°C and the water outlet temperature was 80°C. However, when the water inlet temperature was 40°C, the improvement of COP could be impaired to 12.98%. Through changing the designs of the FTGC with the fixed total heat transfer area, when the water inlet and outlet temperatures were 10°C and 60°C, the highest maximum COP could be obtained with the design used in the experiments.

Keywords

transcritical CO_2 heat pump water heater; fluted tube-in-tube gas cooler; simulation model; coefficient of performance

Nomenclature

Symbols

A	Area [m^2]
c_p	Isobaric specific heat [kJ·(kg·K)$^{-1}$]
D	Diameter [m]
e	Flute depth [m]
e^*	Nondimensional flute depth [-]
f	Frictional factor [-]
h	Enthalpy [kJ·kg^{-1}]
k	Thermal conductivity [W·(m·K)$^{-1}$]
L	Length of tube [m]
m	Mass flow rate [kg·s^{-1}]
N	Number [-]

Nu	Nusselt number [-]
p	Flute pitch [m]
p^*	Nondimensional flute pitch [-]
P	Pressure [MPa]
Pr	Prandtl number [-]
Q	Heat transfer rate [kW]
R	Thermal resistance [$m^2 \cdot K \cdot W^{-1}$]
Re	Reynolds number [-]
T	Temperature [℃]
u	Flow velocity [$m \cdot s^{-1}$]
U	Overall heat transfer coefficient [$W \cdot (m^2 \cdot K)^{-1}$]
V	Displacement [$m^3 \cdot h^{-1}$]
Vol	Volume [m^3]
x	Position [m]
α	Heat transfer coefficient [$W \cdot (m^2 \cdot K)^{-1}$]
δ	Wall thickness [m]
ΔP	Pressure drop [MPa]
ΔT	Temperature difference [K]

η	Efficiency [-]
θ	Helix angle [rad]
θ^*	Nondimensional helix angle [-]
μ	Dynamic viscosity [Pa·s]
ρ	Density [kg·m^{-3}]

Abbreviations

AOP	Above optimal pressure
BOP	Below optimal pressure
COP	Coefficient of performance
EEV	Electronic expansion valve
FTGC	Fluted tube-in-tube gas cooler
OP	Optimal pressure
STGC	Smooth tube-in-tube gas cooler
ZF	Zoom factor

Subscripts

ave	Average
b	Bulk
c	CO_2

CE	Cold end
com	Compressor
d	Discharge
f	Film
flute	Flute
i	Inside
in	Inlet
max	Maximum
o	Outside
opt	Optimal
out	Outlet
p	Pinch point
pc	Pseudo-critical
s	Suction
v	Volumetric
vi	Volume based inner diameter
vo	Volume based outer diameter
w	Water

wall Wall

1. Introduction

More and more attention has been paid to the issues of energy and environment as the improvement of people's living standard (Liu et al., 2019). For space and hot water heating, air source heat pump is an energy-efficient and reliable solution, but most of them are charged with HFC refrigerants, like R410A or R134a (Dai et al., 2020a). The use of HFCs is restricted according to the Kyoto Protocol due to their great adverse effect on the greenhouse effect (Breidenich et al., 1998). For China, the production and consumption of HFCs will be frozen in 2024 and phased down by 80% in 2045. Therefore, it is necessary to look for the replacement of HFCs in the field of air source heat pump (Dai et al., 2019). As a natural refrigerant, CO_2 has attracted attention from researchers and industries in the fields of refrigeration, air conditioning and heat pump due to its non-toxicity, incombustibility, safety, low cost and environmentally benign (Ehsan et al., 2018). Due to the low critical temperature, the transcritical CO_2 cycle is generally applied (Lorentzen and Pettersen, 1993) and recent studies have demonstrated the enormous energy-saving potential by implementing transcritical CO_2 system (Dai et al., 2020b). Especially for the water heating application with a large temperature lift, the transcritical CO_2 cycle presents a unique superiority compared to the traditional HFC refrigerants (Austin and Sumathy, 2011). The temperature glide in the supercritical exothermic process can diminish the entropy generation and enhance the system performance (Zhang et al., 2018).

In CO_2 systems, the gas cooler is an important component that greatly impacts the system efficiency (Yang et al., 2016), and many relevant studies have been carried out. Fronk and Garimella (2011a, b) conducted an experimental and analytical study on microchannel water-CO_2 gas coolers with a general counter-flow configuration. Tsamos et al. (2017) experimentally studied the performance of finned-tube CO_2 gas coolers/condensers with different designs in a CO_2 booster system. Wang et al. (2019a) investigated a compact microchannel gas cooler applied in an automobile CO_2 heat pump system. Then, they also studied the series gas cooler configuration and found that the application of series gas cooler configuration can result in an average 33.7% increase of heating capacity and an average 35% increase of COP (Wang et al., 2019b). Lata and Gupta (2020) adopted a modified evaporative cooling system in gas cooler/condenser of supermarket CO_2 booster refrigeration systems with various configurations. Zendehboudi et al. (2021) researched the heat transfer and pressure drop of brazed plate heat exchangers that belong to a tri-partite CO_2 gas cooler which can simultaneously fulfill the demands of domestic hot water and space heating.

Moreover, the tube-in-tube heat exchanger is a widely used solution for water-CO_2 gas coolers. Yu et al. (2012) modeled a tube-in-tube CO_2 gas cooler and pointed out that the heat transfer of CO_2 near the pseudo-critical region showed a very small temperature variation. Chen (2016) carried out the pinch point analysis for smooth tube-in-tube gas cooler and found the critical flow ratios of water to CO_2 that influence the temperature difference at the pinch point. Zhang et al. (2018) proposed a thermodynamic optimization method based on temperature glide matching and applied it to a CO_2 heat pump water heater using tube-in-tube gas cooler. Yang and Ning (2019) studied the effects of operating parameters on heat transfer performance of evaporator in a transcritical CO_2 heat pump with tube-in-tube gas cooler and evaporator. Peng et al. (2020) developed simulation models of the transcritical CO_2 vapor-injection heat pump system, which utilized tube-in-tube gas cooler and evaporator, and investigated the effect of operating parameters on heating performance.

To improve the performance of the tube-in-tube heat exchanger, some researchers have tried different types of inner tubes, such as multi-twisted tubes (Yang et al., 2016) and corrugated tubes (Ndiaye, 2017). The fluted tube is a type that is extensively used in the design of tubular heat exchangers (Srinivasan and Christensen, 1992). Wang et al. (2000) introduced the carbon steel fluted tube for replacing the copper smooth tube and found that the total heat transfer coefficient of the carbon steel fluted tube was close to that of the copper smooth tube. Zhu et al. (2010), Park (2010) and Wang et al. (2017) numerically investigated the film condensation on fluted tubes. Qi et al. (2017) experimentally studied the characteristics of TiO_2-water nanofluids flowing in a fluted tube and a smooth tube. They found that compared to the laminar flow in the fluted tube, the turbulent flow had a larger increase in heat transfer and a smaller increase in frictional factors. Yu et al. (2020) numerically researched the supercritical CO_2 cooling in the fluted tube and obtained an optimal geometric structure under a certain condition.

In terms of the fluted tube applied in heat exchangers, Rousseau et al. (2003) described a model to simulate fluted tube condenser by using smooth tube correlations combined with the modification based on helical coils and empirical data for fluted tube condensers. For CO_2 gas coolers, the models were mainly built by the segmented method (Li et al., 2017; Qin et al., 2020) and the moving boundary method (Bahman et al., 2020) due to the supercritical CO_2 properties. Xu et al. (2011) developed a segmented CO_2 gas cooler model that consisted of a fluted tube and helically coiled tubes embedded in the groove of the fluted tube. They found that with a decrease of the inner fluted tube diameter, the heating capacity increased and the CO_2 pressure drop changes slightly. Huang et al. (2014) presented a generalized finite volume model for the tube-in-tube heat exchanger. To calculate the two-phase flow in the fluted tube annuli, they applied empirical two-phase flow multipliers onto existing fluted tube single-phase correlations. Chen et al. (2016) proposed helically-coiled fluted tube heat exchangers for use in fluoride-salt-cooled high temperature reactor systems. Zhu et al. (2019) investigated the heat transfer characteristics of supercritical CO_2 cooling in the fluted tube-in-tube heat exchanger and developed a new correlation for it. However, they did not study the influence of the fluted tube-in-tube heat exchanger on the system performance of CO_2 heat pump.

As mentioned above, the fluted tube is a promising solution from the heat transfer improvement point of view, and it has already been applied in some tube-in-tube heat exchangers. However, for the supercritical CO_2 gas cooler, the publication about the application of the fluted tube is still very limited. Moreover, the effect of the higher pressure drop caused by the special geometric structure of the fluted tube on the performance of heat exchanger has not been reported yet. To fill the research gap, a simulation model considering the pressure drop of supercritical CO_2 was developed to investigate the fluted tube-in-tube gas cooler (FTGC). After the model validation, compared to the smooth tube-in-tube gas cooler (STGC) with the same geometric parameters, the effects of different parameters on the heat transfer performance were analyzed. Furthermore, the investigation on the system performance of CO_2 heat pump using the FTGC has not been published as well. Thus, this paper evaluated the COP of systems with FTGC and STGC, and the different designs of the FTGC were calculated to optimize the heat exchanger.

2. Experimental setup

2.1 Tested system

The studied FTGC was installed in a transcritical CO_2 heat pump water heater, which is shown in Fig. 1. The characteristics of the components are displayed in Table 1. The information on the FTGC will be introduced in Section 2.2. Through adjusting the opening of the EEV, the discharge pressure and temperature would accordingly change, which generated different CO_2 inlet conditions of the FTGC. The regulating valve could manipulate the water flow rate to reach the targeted water outlet temperature. The water inlet temperature was controlled by devices of the laboratory.

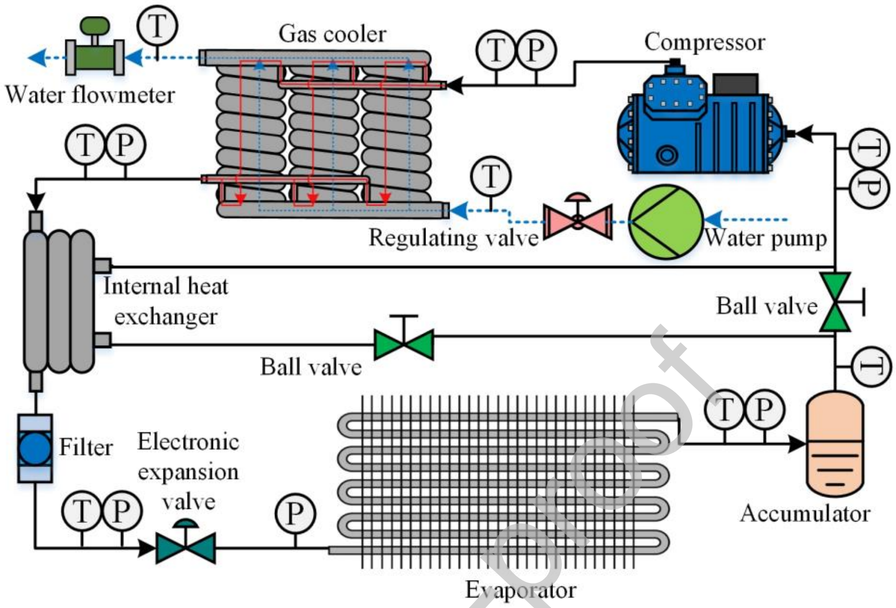

Fig. 1. Schematic of transcritical CO_2 heat pump.

Table 1 Characteristics of the components.

Component	**Characteristic**
Compressor	Type: Semi-hermetic reciprocating
	Rated rotational speed: 1450 rpm
	Rated displacement: 11.69 $m^3 \cdot h^{-1}$
Evaporator	Type: Finned-tube
	Tube: Φ7 mm×0.7 mm copper tube
	Tube length: 1600 mm
	Fin type: Aluminum, Wavy
	Fin spacing: 2.4 mm

	Fin thickness: 0.2 mm Number of heat exchanger: 2 (V-shaped arrangement) Number of rows per heat exchanger: 4 Number of copper tubes per row: 48 Number of refrigerant circuits per heat exchanger: 12
Internal heat exchanger	Type: Fluted tube-in-tube Flow type: Counter flow Outside tube: Φ33 mm×1.5 mm stainless steel tube Inside tube: Fluted copper tube Total heat transfer area: 0.27 m^2
Electronic expansion valve	Type: Stepper motor
Accumulator	Inside volume: 9.5 L

2.2 Fluted tube-in-tube gas cooler

The FTGC was made of three same heat exchangers in parallel. In each heat exchanger, as Fig. 1 shows, the water generally flowed from the bottom to the top along the tube, while the CO_2 flowed from the top to the bottom. The fluted tube-in-tube structure and the key geometric parameters are displayed in Fig. 2. The outer tube was a stainless-steel circular tube with the inner diameter denoted as D_o, and the inner tube was a fluted copper tube. The water and CO_2 flowed in the tube side and the annulus side, respectively.

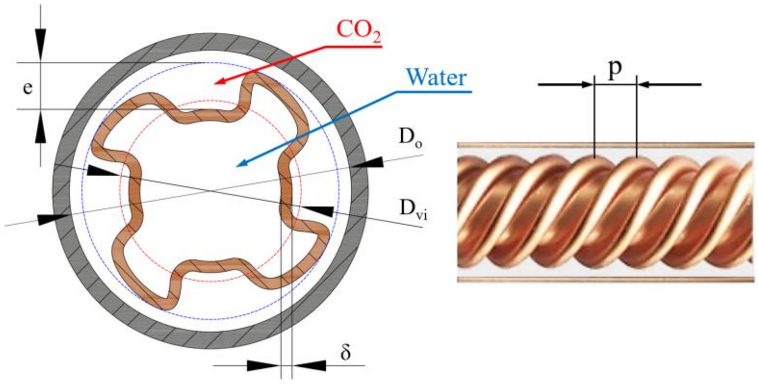

Fig. 2. Details of the fluted tube-in-tube structure.

Due to the complex shape of the fluted tube, the volume based inner diameter D_{vi} was adopted and can be expressed as (Rousseau et al., 2003):

$$D_{\mathrm{vi}} = \sqrt{\frac{4 \cdot Vol}{\pi L}} \tag{1}$$

where *Vol* is the volume enclosed inside the fluted tube. The volume based outer diameter D_{vo} can be calculated as:

$$D_{\mathrm{vo}} = D_{\mathrm{vi}} + 2\delta \tag{2}$$

In terms of the fluted structure, the flute depth e and the flute pitch p are important parameters. The nondimensional parameters (e^* and p^*) are respectively determined by e and p dividing with D_{vi}. The helix angle θ can be calculated by:

$$\theta = arctan\left(\frac{\pi D_{\mathrm{vo}}}{N_{\mathrm{flute}}\, p}\right) \tag{3}$$

where N_{flute} is the number of flutes and equals to 4. The nondimensional helix angle θ^*

is calculated by θ dividing with $\pi/2$. The geometric parameters of the fluted tube-in-tube structure are summarized in Table 2.

Table 2 Geometric parameters of the fluted tube-in-tube structure.

Parameter	**Description**	**Value**
D_o	Inner diameter of outer tube [mm]	25
D_{vi}	Volume based equivalent inner diameter of inner tube [mm]	16.07
D_{vo}	Equivalent outer diameter of inner tube [mm]	18.07
δ	Wall thickness of inner tube [mm]	1
e	Flute depth [mm]	4.16
p	Flute pitch [mm]	13
θ	Helix angle [rad]	0.829
L	Length of tube [m]	18
e^*	Dimensionless flute depth [-]	0.259
p^*	Dimensionless flute pitch [-]	0.809
θ^*	Dimensionless helix angle [-]	0.528
A_i	Inside heat transfer area of the inner tube [m^2]	1.307
A_o	Outside heat transfer area of the inner tube [m^2]	1.421

2.3 Measurement devices

The environmental laboratory, which could provide different ambient temperature and water inlet temperature, consisted of water adjusting system, air adjusting system, electric control system, data acquisition system and environmental room. The positions of the temperature and pressure sensors are shown in Fig. 1. Type T thermocouples and thermal resistances PT100 were adopted. The measurement range of the temperature sensors was -200–350℃, and the accuracy was ±0.2℃. The

CO_2 pressure was measured by pressure transmitters with a measurement range of 0–16 MPa and an accuracy of ±0.25% of full span. The water volumetric flow rate was measured by an electromagnetic flowmeter with a measurement range of 0–6 $m^3 \cdot h^{-1}$ and an accuracy of ±0.5% of full span. When the steady state in which the parameters barely changed for 5 minutes was reached, all the measurements were collected to obtain the performance by time-averaged. The ranges of the experimental parameters are summarized in Table 3.

Table 3 Ranges of the experimental parameters.

Parameter	**Unit**	**Range**
CO_2 inlet pressure	MPa	7.89-12.60
CO_2 inlet temperature	℃	56.75-144.78
CO_2 mass flow rate	$kg \cdot s^{-1}$	0.089-0.405
CO_2 outlet pressure	MPa	7.43-11.83
CO_2 outlet temperature	℃	7.45-55.75
Water inlet temperature	℃	6.93-55.65
Water outlet temperature	℃	42.48-90.78
Water volumetric flow rate	$m^3 \cdot h^{-1}$	0.297-2.390

2.4 Data reduction

The heat transfer rate of the gas cooler can be expressed as:

$$Q_{gc} = m_{\mathrm{w}} c_{\mathrm{pw}} \left(T_{\mathrm{w,out}} - T_{\mathrm{w,in}} \right) \tag{4}$$

Based on the heat transfer balance, the mass flow rate of CO_2 can be determined by:

$$m_{\mathrm{c}} = \frac{Q_{\mathrm{gc}}}{h_{\mathrm{c,in}} - h_{\mathrm{c,out}}} \tag{5}$$

The CO_2 pressure drop can be expressed as:

$$\Delta P_{\mathrm{c}} = P_{\mathrm{c,in}} - P_{\mathrm{c,out}} \tag{6}$$

Based on the method proposed by Moffat (1988), the uncertainty analysis was conducted. The uncertainties of Q_{gc}, m_{c} and ΔP_{c} are 3.59%, 4.22% and 7.86%, respectively.

3. Simulation model

3.1 Correlations used in the simulation model

3.1.1 Water side

For the water heating inside the fluted tube, the correlations from Rousseau et al. (2003) were used. The Nusselt number can be calculated by:

$$Nu_{\mathrm{w}} = \begin{cases} 0.014\, Re_{\mathrm{w}}^{0.842}\, Pr_{\mathrm{w}}^{0.4} (e^*)^{-0.067} (p^*)^{-0.293} (\theta^*)^{-0.705}, & Re_{\mathrm{w}} \le 5000 \\ 0.064\, Re_{\mathrm{w}}^{0.773}\, Pr_{\mathrm{w}}^{0.4} (e^*)^{-0.242} (p^*)^{-0.108} (\theta^*)^{0.599}, & Re_{\mathrm{w}} > 5000 \end{cases} \tag{7}$$

The Reynolds number *Re*, Prandtl number *Pr* and heat transfer coefficient α can be expressed as:

$$Re = \frac{\rho u D}{\mu} \tag{8}$$

$$Pr = \frac{c_{\mathrm{p}}\mu}{k} \tag{9}$$

$$\alpha = \frac{Nuk}{D} \tag{10}$$

The frictional factor can be determined by:

$$f_{\mathrm{w}} = \begin{cases} 0.554\left(\dfrac{64.0}{Re_{\mathrm{w}} - 45.0}\right)(e^{*})^{0.384}(p^{*})^{-1.454+2.083e^{*}}(\theta^{*})^{-2.426} & , Re_{\mathrm{w}} \le 1500 \\ 1.209 Re_{\mathrm{w}}^{-0.261}(e^{*})^{1.26-0.05p^{*}}(p^{*})^{-1.66+2.033e^{*}}(\theta^{*})^{-2.699+3.67e^{*}} & , Re_{\mathrm{w}} > 1500 \end{cases} \tag{11}$$

For the water flowing inside the smooth tube, the correlation from Gnielinski (1976) was adopted:

$$Nu_{\mathrm{w}} = \frac{(f_{\mathrm{w}}/8)(Re_{\mathrm{w}} - 1000)Pr_{\mathrm{w}}}{1 + 12.7(f_{\mathrm{w}}/8)^{1/2}\left(Pr_{\mathrm{w}}^{2/3} - 1\right)} \tag{12}$$

$$f_{\mathrm{w}} = \left(1.82 \log Re_{\mathrm{w}} - 1.64\right)^{-2} \tag{13}$$

3.1.2 Supercritical CO_2 side

For the supercritical CO_2 cooling and flowing in the fluted annulus, the Nusselt number can be calculated based on the correlation from Zhu et al. (2019):

$$Nu_{\mathrm{b}} = \begin{cases} 1.85 Nu_0 \left(\dfrac{Pr_{\mathrm{b}}}{Pr_{\mathrm{wall}}} \right)^{1.5128} \left(\dfrac{\rho_{\mathrm{b}}}{\rho_{\mathrm{wall}}} \right)^{-0.7115} \left(\dfrac{c_{\mathrm{p,b}}}{\overline{c}_{\mathrm{p}}} \right)^{-2.2726} \left(\dfrac{D_{\mathrm{vo}}}{p} \right)^{0.447}, T_{\mathrm{b}} \le T_{\mathrm{pc}} \\ 3.7 Nu_0 \left(\dfrac{Pr_{\mathrm{b}}}{Pr_{\mathrm{wall}}} \right)^{0.0479} \left(\dfrac{\rho_{\mathrm{b}}}{\rho_{\mathrm{wall}}} \right)^{0.9577} \left(\dfrac{c_{\mathrm{p,b}}}{\overline{c}_{\mathrm{p}}} \right)^{-0.2729} \left(\dfrac{D_{\mathrm{vo}}}{p} \right)^{0.447}, T_{\mathrm{b}} > T_{\mathrm{pc}} \end{cases} \tag{14}$$

where Nu_0 is calculated using the correlations from Gnielinski (1976) as shown in equation (12). The averaged specific heat $\overline{c}_{\mathrm{p}}$ can be determined by:

$$\overline{c}_{\mathrm{p}} = \frac{\int_{T_{\mathrm{b}}}^{T_{\mathrm{wall}}} c_{\mathrm{p}} dT}{T_{\mathrm{wall}} - T_{\mathrm{b}}} = \frac{h_{\mathrm{wall}} - h_{\mathrm{b}}}{T_{\mathrm{wall}} - T_{\mathrm{b}}} \tag{15}$$

With the best knowledge of the authors, there is no correlation for the frictional factor of supercritical CO_2 flowing in the fluted annulus. Therefore, a correlation was proposed based on the experimental data:

$$f_{\mathrm{c}} = \left(0.653 \, log \, Re_{\mathrm{b}} - 2.415\right)^{-2.537} \tag{16}$$

For the supercritical CO_2 cooling in the smooth annulus, the correlation from Dang and Hihara (2004) was used:

$$Nu_{\mathrm{b}} = \frac{\left(f_{\mathrm{c}}/8\right)\left(Re_{\mathrm{b}} - 1000\right) Pr_{\mathrm{c}}}{1.07 + 12.7\left(f_{\mathrm{c}}/8\right)^{1/2}\left(Pr_{\mathrm{c}}^{2/3} - 1\right)} \tag{17}$$

$$Pr_{\mathrm{c}} = \begin{cases} c_{\mathrm{p,b}} \mu_{\mathrm{b}} / k_{\mathrm{b}}, \ for \ \mathrm{c}_{\mathrm{p,b}} \ge \overline{c}_{\mathrm{p}} \\ \overline{c}_{\mathrm{p}} \mu_{\mathrm{b}} / k_{\mathrm{b}}, \ for \ \mathrm{c}_{\mathrm{p,b}} < \overline{c}_{\mathrm{p}} \text{ and } \mu_{\mathrm{b}} / k_{\mathrm{b}} \ge \mu_{\mathrm{f}} / k_{\mathrm{f}} \\ \overline{c}_{\mathrm{p}} \mu_{\mathrm{f}} / k_{\mathrm{f}}, \ for \ \mathrm{c}_{\mathrm{p,b}} < \overline{c}_{\mathrm{p}} \text{ and } \mu_{\mathrm{b}} / k_{\mathrm{b}} < \mu_{\mathrm{f}} / k_{\mathrm{f}} \end{cases} \tag{18}$$

$$f_{\mathrm{c}} = \left(1.82 \, log \, Re_{\mathrm{f}} - 1.64\right)^{-2} \tag{19}$$

$$Re_{\mathrm{b}} = \frac{\rho_{\mathrm{b}} u D}{\mu_{\mathrm{b}}} \tag{20}$$

$$Re_{\mathrm{f}} = \frac{\rho_{\mathrm{b}} u D}{\mu_{\mathrm{f}}} \tag{21}$$

where the subscript f denotes the film temperature, and the film temperature is the average of wall temperature and bulk temperature.

3.2 Calculation method

In the gas cooler, the heat transfer happens with significant changes of temperature and thermodynamic properties. To ensure the calculation accuracy, the gas cooler was divided into a series of segments with the same length for the simulation (Yu et al., 2012). The thermophysical properties of CO_2 and water were calculated based on NIST REFPROP 9.1 (Lemmon et al., 2013). The simulation model was programed in the MATLAB.

The following assumptions were adopted:

(1) The flows were considered as homogeneous and one-dimensional steady;

(2) The heat loss to the ambient air was neglected;

(3) The thermal conduction in the axis direction of the tube was ignored;

(4) The pressure drops caused by the gravitation and the ports were neglected.

Fig. 3 shows the flow chart of the model calculation method. After the input of the condition parameters of CO_2 and water and the geometric parameters of the heat exchanger, the states at the hot end, i.e. the CO_2 inlet and water outlet of the first segment, could be determined. After that, the water mass flow rate was assumed. Then, for each segment, the heat transfer coefficients and the frictional factors of water and CO_2 side was obtained based on equation (7) - (21). The overall $(UA)_j$ can be obtained by:

$$\left(UA\right)_{\mathrm{j}} = \frac{1}{\dfrac{1}{\alpha_{\mathrm{c,j}}A_{\mathrm{o,j}}} + R_{\mathrm{i,j}} + \dfrac{ln\left(D_{\mathrm{vo}} / D_{\mathrm{vi}}\right)}{2\pi k_{\mathrm{wall}} L_{\mathrm{j}}} + R_{\mathrm{o,j}} + \dfrac{1}{\alpha_{\mathrm{w,j}}A_{\mathrm{i,j}}}} \tag{22}$$

where $R_{i,j}$ and $R_{o,j}$ are the thermal resistances caused by inner and outer fouling of the fluted tube. The local heat transfer rate at each segment Q_j can be expressed as:

$$Q_{\mathrm{j}} = \left(UA\right)_{\mathrm{j}} \Delta T_{\mathrm{j}} \tag{23}$$

The states at the CO_2 outlet of the j^{th} segment can be determined based on the heat transfer balance:

$$Q_{\mathrm{j}} = m_{\mathrm{c}}\left(h_{\mathrm{c,in,j}} - h_{\mathrm{c,out,j}}\right) = m_{\mathrm{w}} c_{\mathrm{pw}}\left(T_{\mathrm{w,out,j}} - T_{\mathrm{w,in,j}}\right) \tag{24}$$

During the in-sequence calculation of the segments, if the water inlet temperature of the j^{th} segment was lower than the input water inlet temperature, the calculation could be immediately stopped and iterated with a larger water mass flow rate. When the states of all segments were obtained, comparing the calculated and input water inlet temperature of the gas cooler, the water mass flow rate was iterated until the error was acceptable. Finally, the CO_2 outlet parameters, water mass flow rate and temperature profiles could be output.

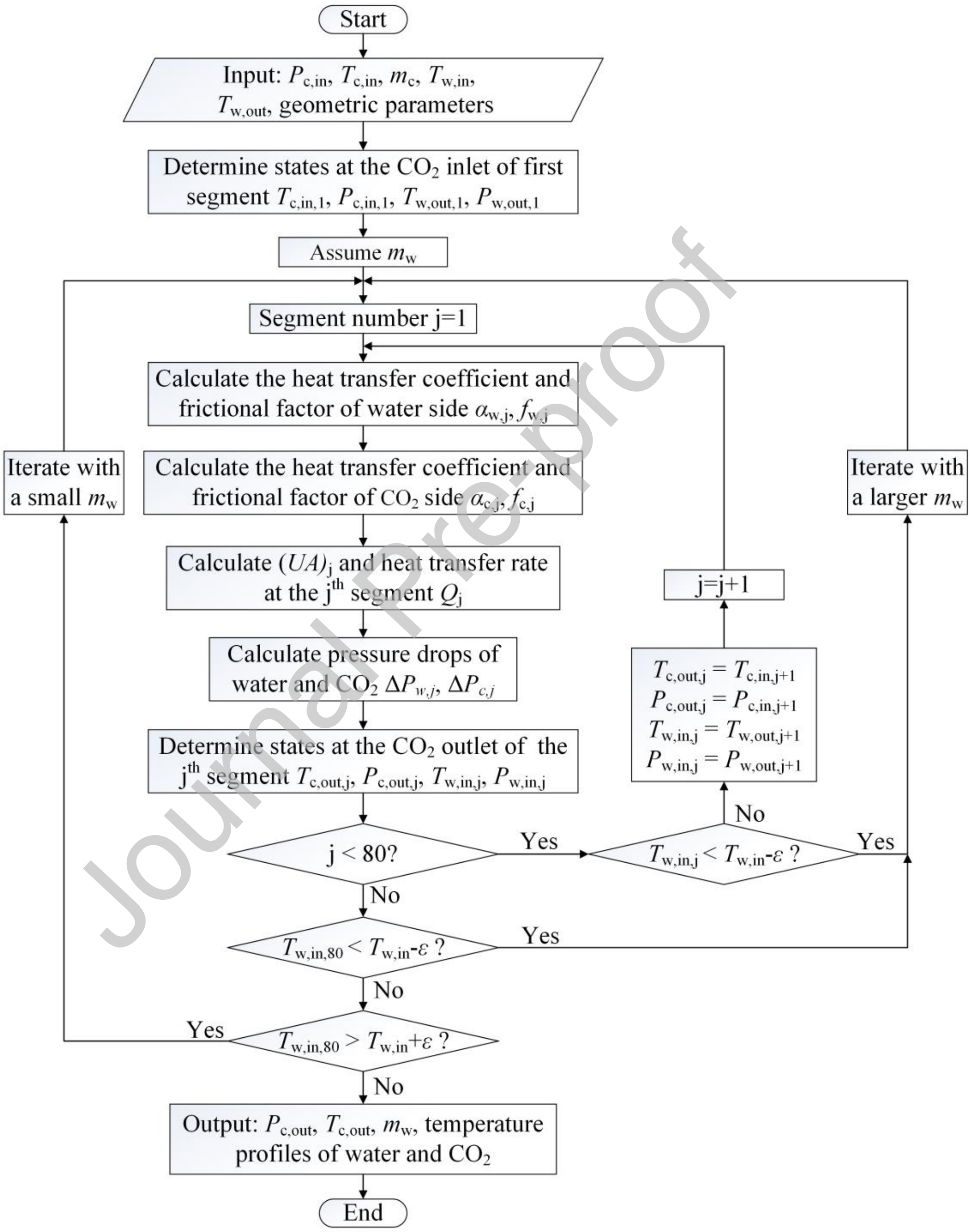

Fig. 3. The flow chart of the model calculation method.

Although the calculation would be more accurate when the number of segments was very large, the calculation time accordingly increased. To determine the number of segments, a sensitivity analysis was conducted. Fig. 4 shows the variations of calculated results with the increase of segment number in the FTGC. When the number was large, the variations of results were slight. The relative deviation of heat transfer rate was 0.142% when the results with the segment number of 80 and 110 were compared. In this paper, the segment number of 80 was used to balance the time and accuracy.

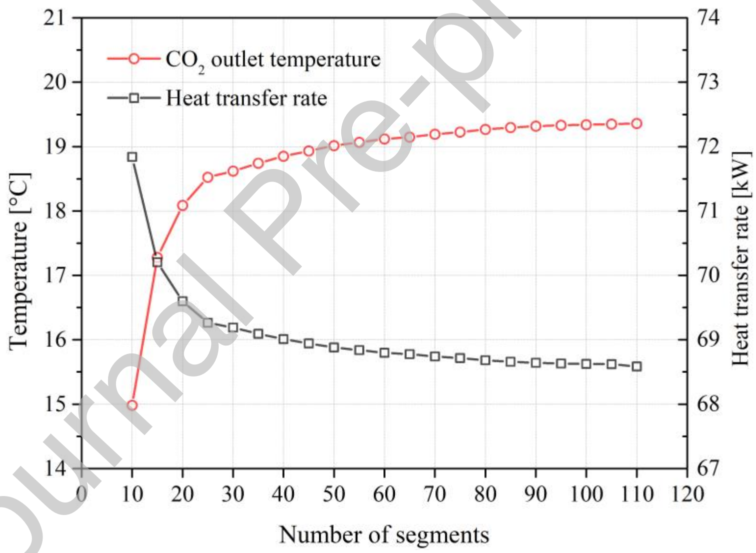

Fig. 4. Variations of calculated CO_2 outlet temperature and heat transfer rate in the FTGC with the increase of segment number.

3.3 Model validation

The comparison between the experimental and calculated heat transfer rates of the FTGC is shown in Fig. 5. The CO_2 inlet pressure, CO_2 inlet temperature, CO_2

mass flow rate, water inlet temperature and water outlet temperature were the input, while the CO_2 outlet pressure, CO_2 outlet temperature and water flow rate were the output. As shown in Fig. 5, the calculated values agreed with the experimental values within an error of 8%. Regarding the output parameters, the absolute mean relative errors of the CO_2 outlet pressure and the water flow rate were 1.99% and 2.95%, respectively; the absolute mean error of the CO_2 outlet temperature was 1.14 K. Hence, the simulation model could obtain the results with acceptable accuracy and could be applied for further investigation. As for the validation of the STGC model, the correlations used in the STGC model were commonly used in the literature (Li et al., 2013; Minetto, 2011; Yang et al., 2016; Yu et al., 2012; Zhu et al., 2019), and the reliability of the model has been verified by them.

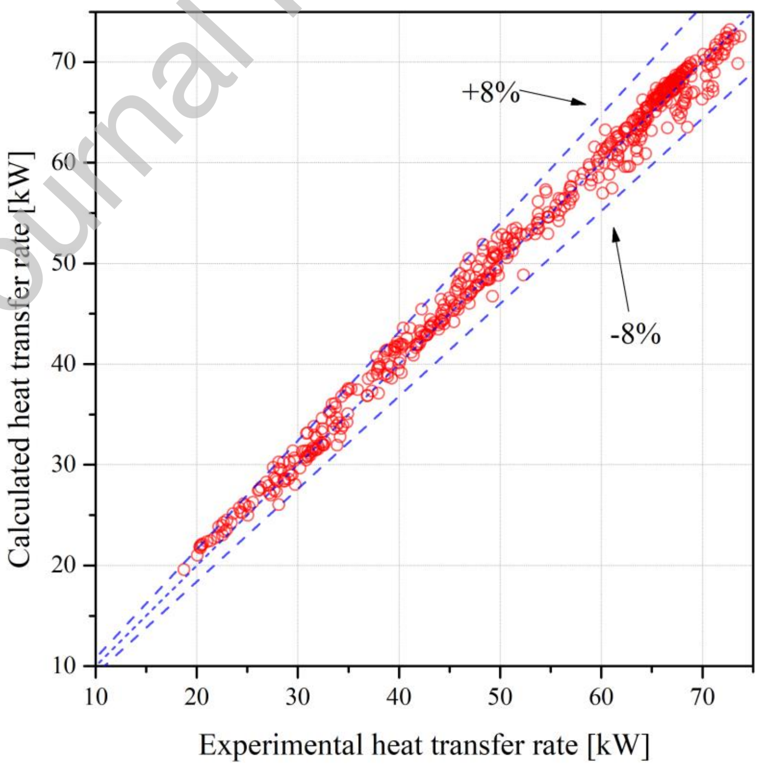

Fig. 5. Comparison between the experimental and calculated heat transfer rates of the FTGC.

4. Results and discussion

4.1 Effects of different parameters on the heat transfer performance

In this section, the performance of the FTGC was analyzed through simulation. Besides, the STGC with the same geometric parameters was also simulated to show the difference.

4.1.1 CO_2 side conditions

Fig. 6 shows the temperature profiles of CO_2 and water along the length of the heat transfer tube under different CO_2 inlet pressures ($P_{c,in}$). The positions of pinch points, where the temperature difference between CO_2 and water reached the minimum, are displayed. The temperature differences at the cold end (ΔT_{CE}) are also shown. Since the water mass flow rate was iterated to match the temperature lift, the ratio of mass flow rate (m_c/m_w) is used to denote the condition of water mass flow rate.

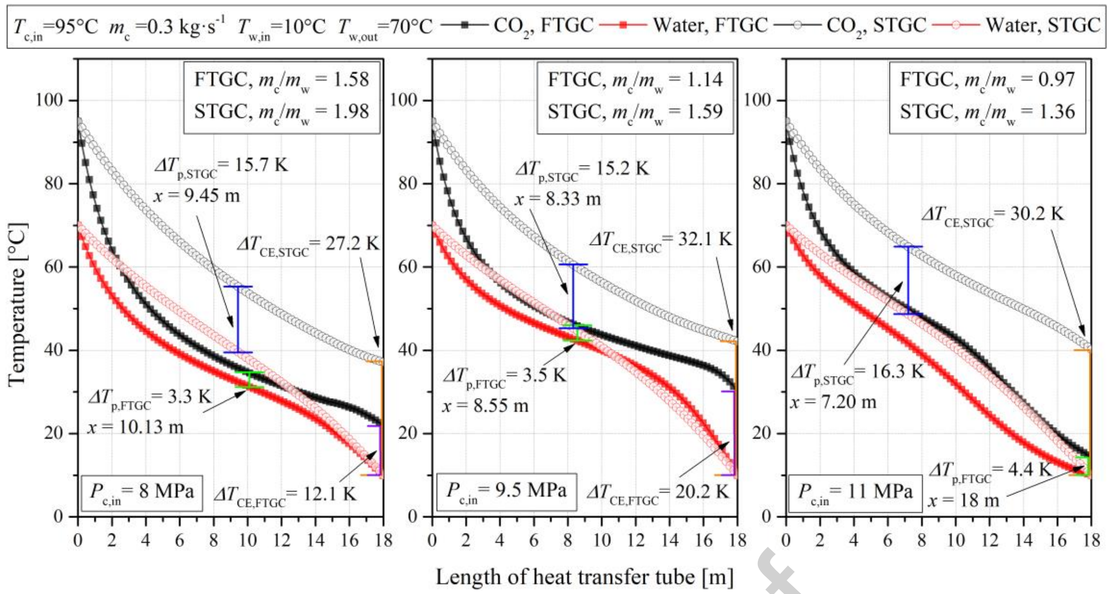

Fig. 6. Temperature profiles of CO_2 and water along the length of the heat transfer tube under different CO_2 inlet pressures.

The CO_2 temperature decreased fast near the CO_2 inlet because of the large temperature difference and lower specific heat. In the FTGC, the heat transfer coefficients in both water and CO_2 sides were improved, and thus the CO_2 temperature was cooled down more and the CO_2 outlet temperature ($T_{c,out}$) was always lower than that in STGC. It could be found that the temperature difference at the pinch point (ΔT_p) in the FTGC was significantly lower than that in the STGC. In the FTGC, the pinch point moved to the cold end when $P_{c,in}$ increased to 11 MPa, which was the desired situation to maximize the enthalpy difference of the gas cooler and achieve the high COP in the CO_2 heat pump (Ye et al., 2020).

Fig. 7 shows the temperature profiles under different CO_2 inlet temperatures ($T_{c,in}$). With the increase of $T_{c,in}$, the decrease of CO_2 temperature near the CO_2 inlet was more rapid due to the increase of temperature difference and the decrease of specific heat. However, the CO_2 temperature curves on the subsequent heat transfer process were similar under different $T_{c,in}$. It indicated that $T_{c,in}$ mainly influenced the temperature profiles near the hot end. In both FTGC and STGC, ΔT_p increased with the increase of $T_{c,in}$. In addition, the pinch point in the STGC moved toward the hot end as $T_{c,in}$ increased; while the pinch point in the FTGC basically located at the middle of the heat transfer tube.

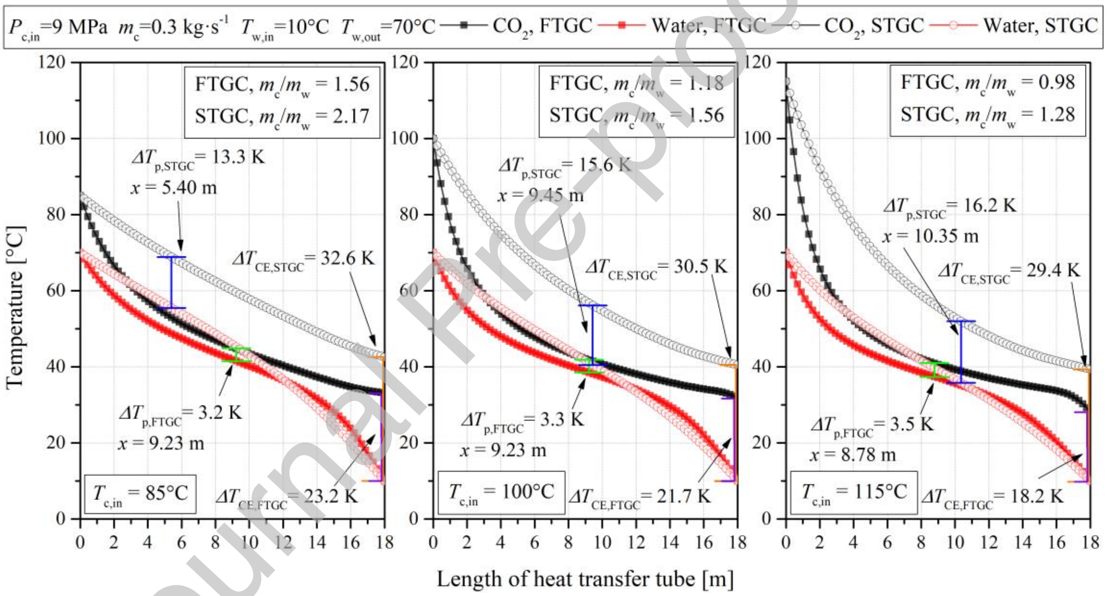

Fig. 7. Temperature profiles of CO_2 and water along the length of the heat transfer tube under different CO_2 inlet temperatures.

Fig. 8 shows the temperature profiles under different CO_2 mass flow rates (m_c). It could be seen that the change of m_c had no significant influence on the temperature profiles in the STGC. As for the FTGC, the effect was obvious near the cold end. ΔT_p increased with the increase of m_c, but the position of the pinch point was slightly affected by m_c. On one hand, the increase of m_c enhanced the heat transfer coefficients; on the other hand, the higher m_c also enlarged the heat capacity, which required more heat transfer rate for the same temperature change. Hence, the combined effect of the heat transfer coefficients and the specific heat capacity made the temperature profiles change insignificantly.

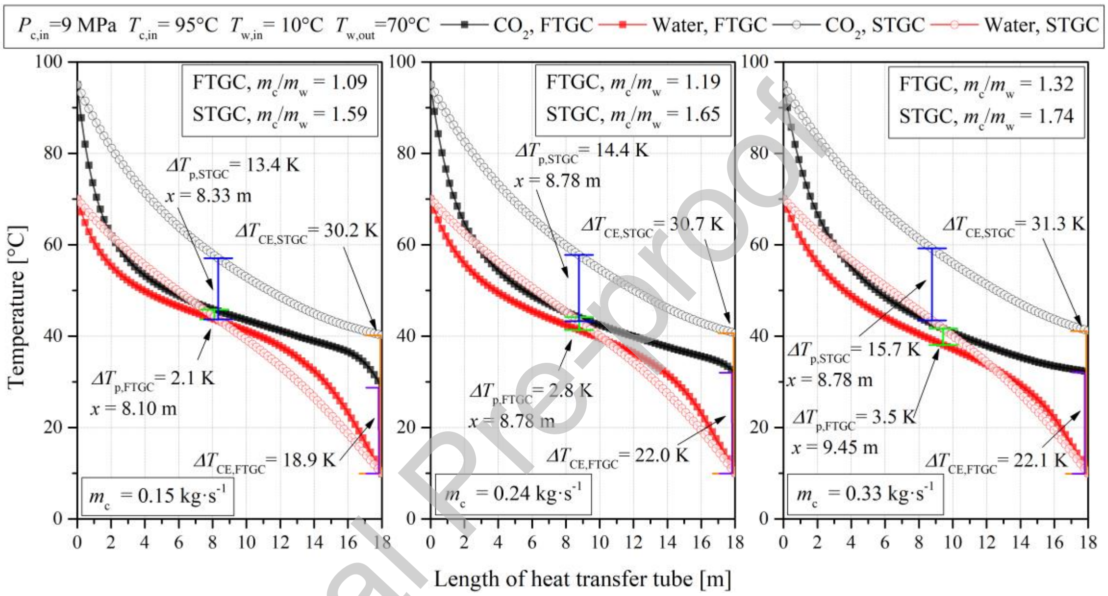

Fig. 8. Temperature profiles of CO_2 and water along the length of the heat transfer tube under different CO_2 mass flow rates.

Fig. 9 shows the variations of the heat transfer rate (Q_h), $T_{c,out}$ and CO_2 outlet pressure ($P_{c,out}$) with the changes of $P_{c,in}$, $T_{c,in}$ and m_c. When $P_{c,in}$ was relatively low, $T_{c,out}$ in both FTGC and STGC was at a high level (respectively up to 32.4℃ and 42.4℃) that was significantly higher than the water inlet temperature $T_{w,in}$. This was because the pinch point occurred in the middle part of the heat exchanger and constrained the cooling down of CO_2. With the increase of $P_{c,in}$, Q_h first increased and then decreased. Moreover, Q_h of FTGC was always higher than that of STGC, and the maximum Q_h of FTGC was 31.2% higher than that of STGC. It proved the heat transfer improvement of the fluted geometry. But the fluted geometry also led to a larger pressure drop, which could be seen from the lower $P_{c,out}$ in the FTGC.

With the increase of $T_{c,in}$, Q_h increased with an approximately linear trend due to the increase of CO_2 inlet enthalpy. $T_{c,out}$ reduced, which could also benefit to the improvement of Q_h, because the increase of $T_{c,in}$ enhanced the heat transfer temperature difference and the water mass flow rate, and then accelerated the cooling of CO_2 from the inlet. For instance, the positions in which the CO_2 temperature in the FTGC reached 40℃ in Fig. 7 were respectively 12.22 m, 10.52 m and 9.46 m at $T_{c,in}$ of 85℃, 100℃ and 115℃. More portion of the heat transfer tube could be used for further cooling when $T_{c,in}$ was higher.

As m_c increased, $T_{c,out}$ marginally increased in the STGC. In the FTGC, although $T_{c,out}$ showed a trend with increase first and then decrease, the change was still small. Q_h showed a proportional increase with the increase of m_c. Besides, there was an obvious decrease of $P_{c,out}$ in the FTGC with the increase of m_c, i.e. the CO_2 pressure drop in the FTGC significantly increased. When m_c increased from 0.15 $kg{\cdot}s^{-1}$ to 0.30 $kg{\cdot}s^{-1}$, the CO_2 pressure drop in the FTGC increased by 123.6%.

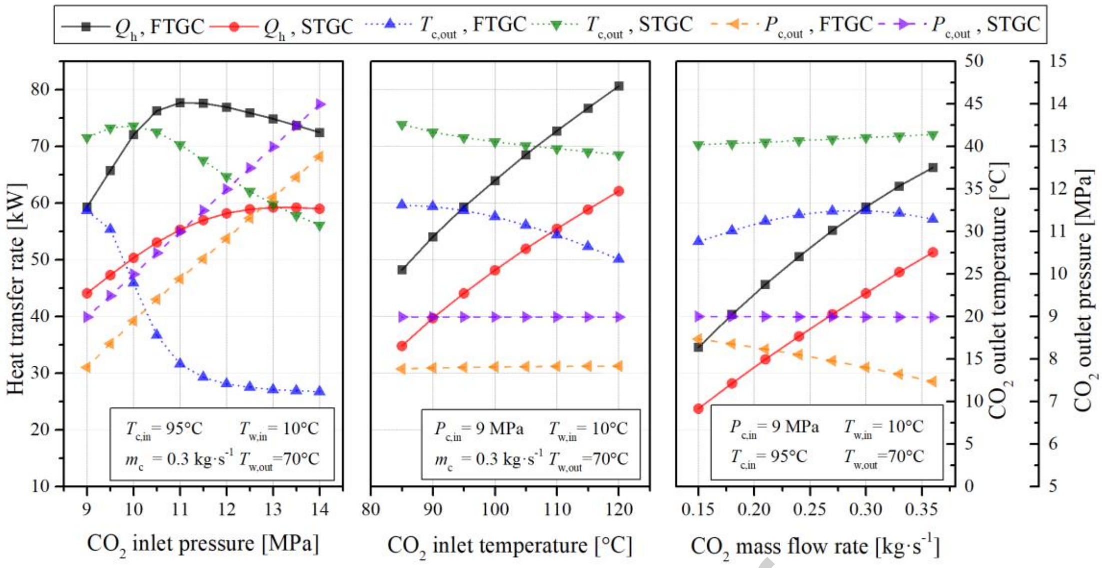

Fig. 9. Variations of the heat transfer rate, CO_2 outlet temperature and CO_2 outlet pressure with the changes of CO_2 inlet pressure, CO_2 inlet temperature and CO_2 mass flow rate.

4.1.2 Water side conditions

Fig. 10 shows the temperature profiles under different $T_{w,in}$. When $T_{w,in}$ was higher, the water temperature changed with a lower speed in the STGC; while the change of water temperature near the cold end declined in the FTGC. The increase of $T_{w,in}$ also reduced the cooling down of CO_2. For example, the positions where the CO_2 in the FTGC reached 40℃ were 10.77 m, 11.39 m and 12.35 m at the $T_{w,in}$ of 5℃, 20℃ and 35℃, respectively. Regarding the position of the pinch point, in both FTGC and STGC, the pinch point moved toward the cold end as $T_{w,in}$ increased. Furthermore, ΔT_p obviously reduced and even reached 0.6 K in the FTGC when $T_{w,in}$ was 35℃.

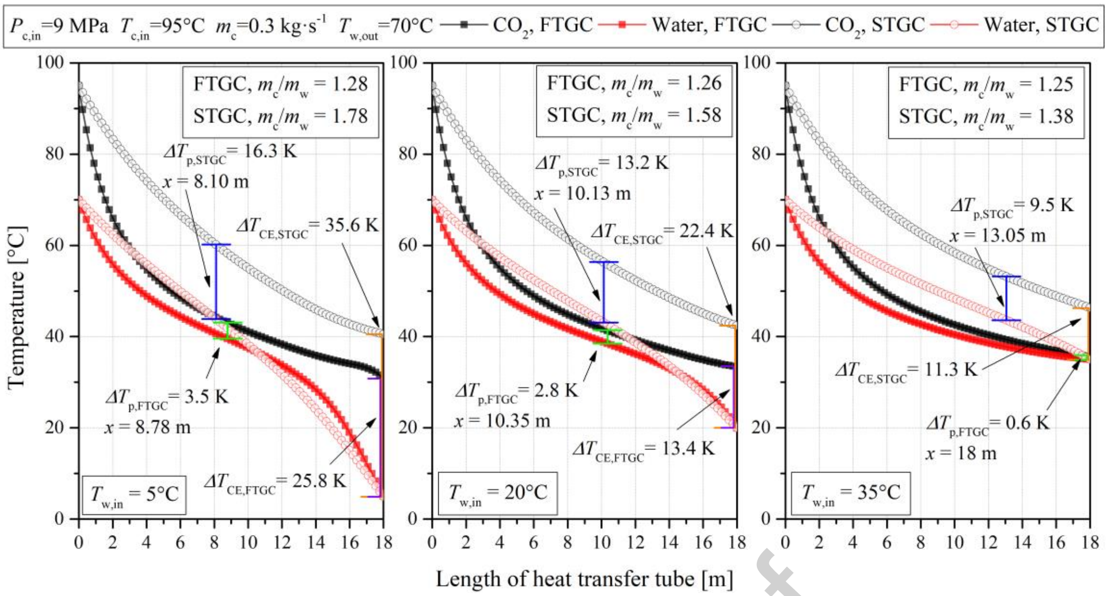

Fig. 10. Temperature profiles of CO_2 and water along the length of the heat transfer tube under different water inlet temperatures.

Fig. 11 shows the temperature profiles under different $T_{w,out}$. The temperature profiles varied more complicatedly when $T_{w,out}$ was low. The significant change of specific heat of supercritical CO_2 with the change of temperature made the temperature show a strongly nonlinear trend. When $T_{w,out}$ was 45°C, the pinch points in FTGC and STGC were at the cold end, and ΔT_p was lower than the values under higher $T_{w,out}$. As $T_{w,out}$ increased, the pinch point moved to the inside of the heat transfer tube.

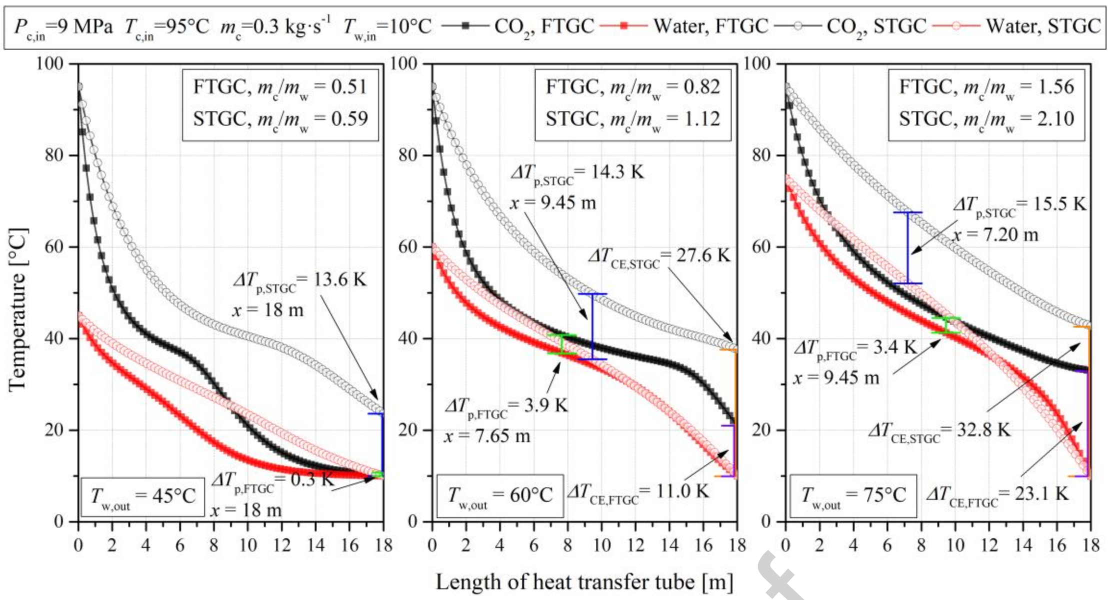

Fig. 11. Temperature profiles of CO_2 and water along the length of the heat transfer tube under different water outlet temperatures.

Fig. 12 displays the variations of of Q_h, $T_{c,out}$ and $P_{c,out}$ with the changes of $T_{w,in}$ and $T_{w,out}$. The varying trend of $T_{c,out}$ was different from that of ΔT_{CE} when $T_{w,in}$ was changing. An line for $T_{w,in}$ is added in Fig. 12 to show ΔT_{CE} better. With the increase of $T_{w,in}$, $T_{c,out}$ increased and ΔT_{CE} decreased. When $T_{w,in}$ was larger than 35℃, $T_{c,out}$ in the FTGC was very close to $T_{w,in}$. It indicated that the FTGC had a superfluous heat transfer capacity when $T_{w,in}$ was high. Q_h decreased with the increase of $T_{w,in}$. When $T_{w,in}$ was 10℃, Q_h in the FTGC was 34.47% higher than that in the STGC. However, as $T_{w,in}$ increased, the difference between Q_h in FTGC and STGC dropped. Moreover, when $T_{w,in}$ was 45℃, Q_h in FTGC was even 0.09% lower than that in STGC. It suggested that the benefit of the higher heat transfer coefficients in the FTGC was suppressed when the maximum possible heat transfer rate was small. Furthermore, the higher pressure drop in the FTGC would lead to a lower Q_h than that in the STGC when $T_{w,in}$ increased further. With the increase of $T_{w,out}$, $T_{c,out}$ increased and Q_h decreased. When $T_{w,out}$ was low (45-55°C), Q_h in the FTGC decreased more slowly because the pinch point located at the cold end and $T_{c,out}$ was close to $T_{w,in}$.

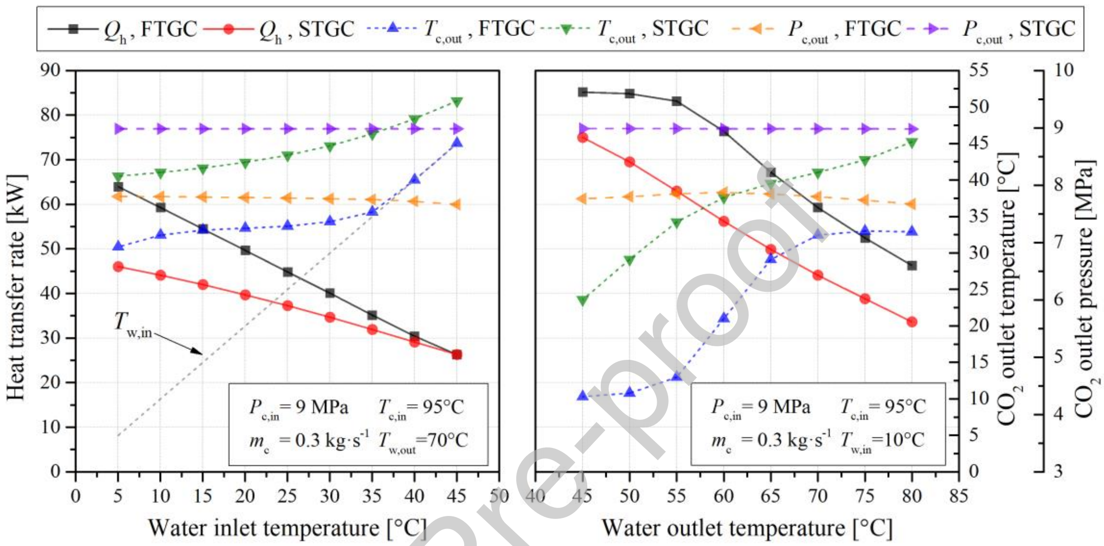

Fig. 12. Variations of the heat transfer rate, CO_2 outlet temperature and CO_2 outlet pressure with the changes of water inlet and outlet temperatures.

4.2 System COP under different conditions

The performance of FTGC and STGC was analyzed above, but the impact on the system COP was also an important issue that should be considered. In this section, the thermodynamic analysis was conducted to study the COP of transcritical CO_2 heat pump cycle without internal heat exchanger under different conditions. During the thermodynamic analysis, the evaporation temperature was 0°C; the superheat degree was 5 K; the throttling process was considered as isenthalpic; the displacement of the compressor was set as 11.69 $m^3 \cdot h^{-1}$ which was the rated value in the tested system; the isentropic and volumetric efficiencies were from Wang et al. (2013). The COP can be defined as:

$$COP_H = \frac{h_{\text{gc,in}} - h_{\text{gc,out}}}{h_{\text{com,out}} - h_{\text{com,in}}} \tag{25}$$

4.2.1 System COP with FTGC and STGC

Fig. 13 shows the variation of COP at $T_{\text{w,in}}$ of 10°C and 40°C. The COP first increased and then decreased with the increase of compressor discharge pressure (P_{d}). Therefore, there was optimal discharge pressure (P_{opt}) for maximizing COP. At the same condition, the COP with FTGC was higher than that with STGC, except when $T_{\text{w,in}}$ was 40°C, $T_{\text{w,out}}$ was 60°C and P_{d} was lower than 9.4 MPa. The exceptional condition was because the large pressure drop in the FTGC increased the CO_2 outlet enthalpy of gas cooler and limited the heating capacity. When $T_{\text{w,in}}$ was 10°C, the maximum COP with FTGC was 27.57% and 29.41% higher than that with STGC at $T_{\text{w,out}}$ of 60°C and 80°C, respectively; While when $T_{\text{w,in}}$ was 40°C, the improvement reduced (6.30% and 12.98% at $T_{\text{w,out}}$ of 60°C and 80°C). Moreover, P_{opt} with FTGC was lower than that with STGC because the larger temperature difference in the STGC required higher P_{d} to make the pinch point move to the cold end, where the CO_2 gas cooler outlet temperature was close to $T_{\text{w,in}}$ and the system COP could be optimized (Chen, 2019).

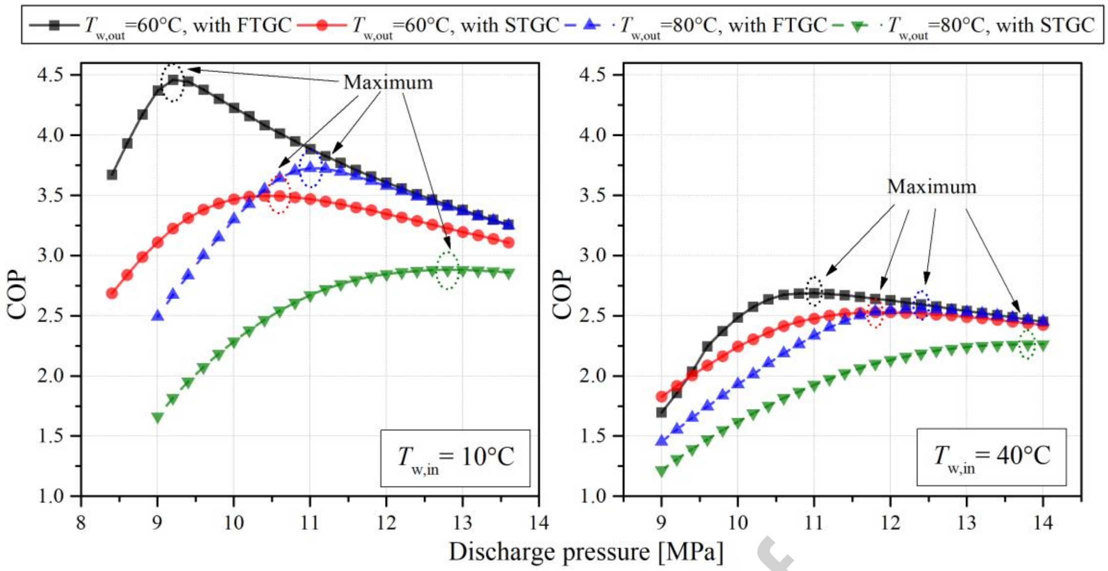

Fig. 13. Variation of COP with the change of discharge pressure at water inlet temperature of 10℃ and 40℃.

Fig. 14 shows the system cycles under the situations of below optimal pressure (BOP), optimal pressure (OP) and above optimal pressure (AOP) at $T_{w,in}$ of 10℃. It could be noticed that the gas cooler outlet temperature decreased as P_d increased. This reduction was more significant in the system with FTGC. The larger reduction of gas cooler outlet temperature was the reason why the COP with FTGC increased faster in Fig. 13. However, because the gas cooler outlet temperature was close to $T_{w,in}$ at P_{opt}, the heating capacity could not further increase, which resulted in the larger decrease of COP. Besides, from the process line of the gas cooler, it could be seen that the pressure drop in the FTGC was obviously higher than that in the STGC, which was the side effect of the enhanced heat transfer caused by the complex structure.

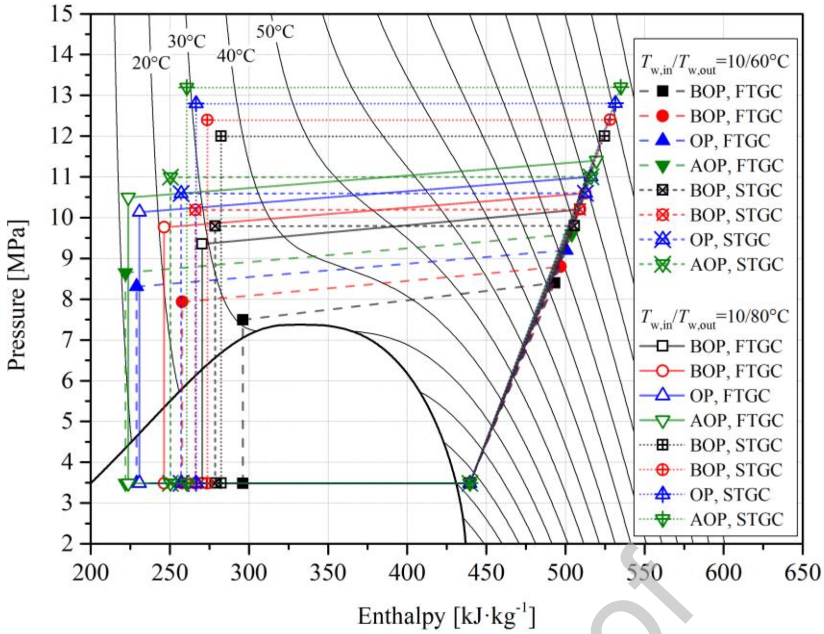

Fig. 14. System cycles at the water inlet temperature of 10℃.

4.2.2 System with different designs of the FTGC

Although the benefit of the FTGC to the system COP was proved, the pressure drop of FTGC was an issue that can be investigated to improve the system performance. In the FTGC, the number of parallel heat exchangers ($N_{parallel}$) and the tube diameter influences the pressure drop, which was discussed in this section.

Fig. 15 shows the COP with FTGC that had various $N_{parallel}$. The condition at low $T_{w,in}$ was chosen because the heat transfer capacity of FTGC was not excessive in this case. Two situations were considered: (1) fixed total heat transfer area and (2) fixed tube length of parallel heat exchangers (18 m). In situation 1, to maintain the same heat transfer area, the length of tube was accordingly changed when $N_{parallel}$ changed; while in situation 2, the total heat transfer area varied with the change of $N_{parallel}$. The increase of $N_{parallel}$ reduces the CO_2 mass flow rate and flow velocity in each heat exchanger and decrease the pressure drop and heat transfer coefficient at the same time. When $N_{parallel}$ increased from 3 to 6 with fixed total heat transfer area at $T_{w,out}$ of 60℃ and P_d of 10 MPa, the pressure drop decreased from 0.99 MPa to 0.29 MPa. With the fixed total heat transfer area, the maximum COP was highest (COP_{max} = 4.46) when $N_{parallel}$ equaled to 3 at $T_{w,out}$ of 60℃; while at $T_{w,out}$ of 80℃, the highest maximum COP (COP_{max} = 3.75) was obtained with $N_{parallel}$ of 2. When $N_{parallel}$ increased to more than 3, the maximum COP kept decreasing. For example, at $T_{w,out}$ of 60℃, the maximum COP decreased from 4.46 to 4.17 when $N_{parallel}$ increased from 3 to 6. It suggested that the advantage of reducing pressure drop could not neutralize the influence of decreasing heat transfer coefficient. However, when the tube length of parallel heat exchangers was fixed, the maximum COP increased with the increase of $N_{parallel}$, but the improvement reduced with the increase of $N_{parallel}$ as well. Compared to that with $N_{parallel}$ of 2, the maximum COP with $N_{parallel}$ of 6 was 11.18% and 9.03% higher at $T_{w,out}$ of 60℃ and 80℃, respectively.

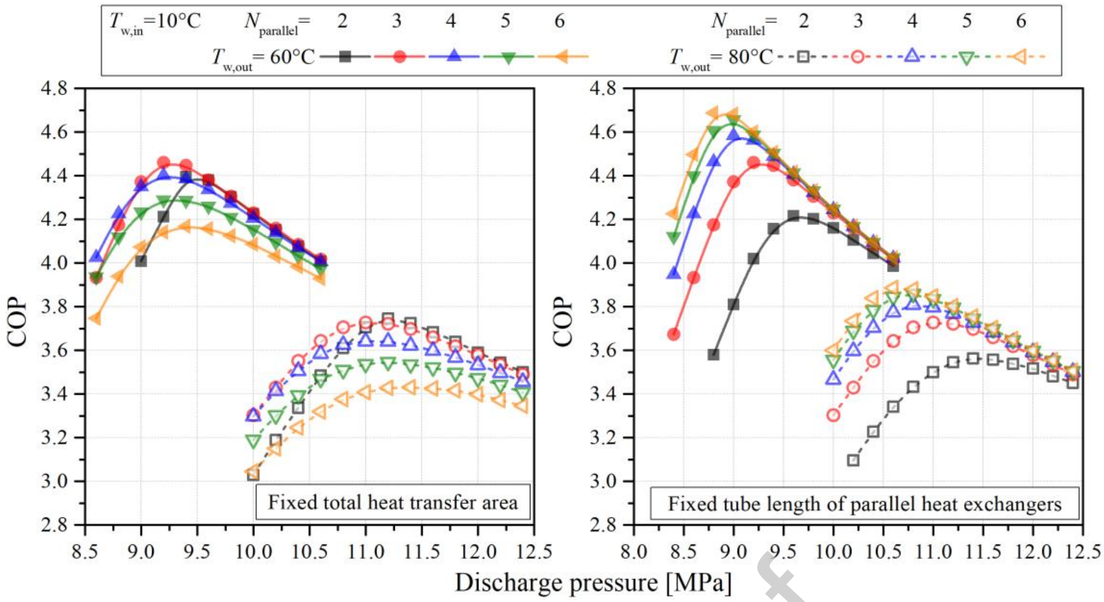

Fig. 15. COP of system with FTGC that had various numbers of parallel heat exchangers.

Fig. 16 displays the COP of system with FTGC that had various zoom factors of tube diameter. Since the simulation model was only validated based on the experimental data with the shape shown in Fig. 2, the zoom factor (ZF) was adopted to study the effect of tube diameter with the same cross-section shape. The cross-section was zoomed up and down with a scale of ZF but the shape was not changed. When $T_{w,out}$ was 60°C with fixed total heat transfer area, the highest maximum COP (COP_{max} = 4.46) was achieved at ZF of 1.0. Compared to those with ZFs of 0.8 and 1.2, the maximum COP with ZF of 1.0 was higher by 2.31% and 1.96%, respectively. When $T_{w,out}$ was 80°C, the ZF of 0.9 showed the best maximum COP (COP_{max} = 3.74). Therefore, when $T_{w,out}$ was 80°C with fixed total heat transfer area, it was beneficial for improving the maximum COP to increase the heat transfer coefficient in spite of the increase of pressure drop through reducing $N_{parallel}$ and ZF slightly. Besides, similar to the effect of $N_{parallel}$, the increase of ZF with the fixed tube length could improve the maximum COP but the improvement declined evidently. The maximum COP with ZF of 1.2 was 5.27% and 2.45% higher than that with ZF of 0.8 when $T_{w,out}$ was 60°C and 80°C, respectively.

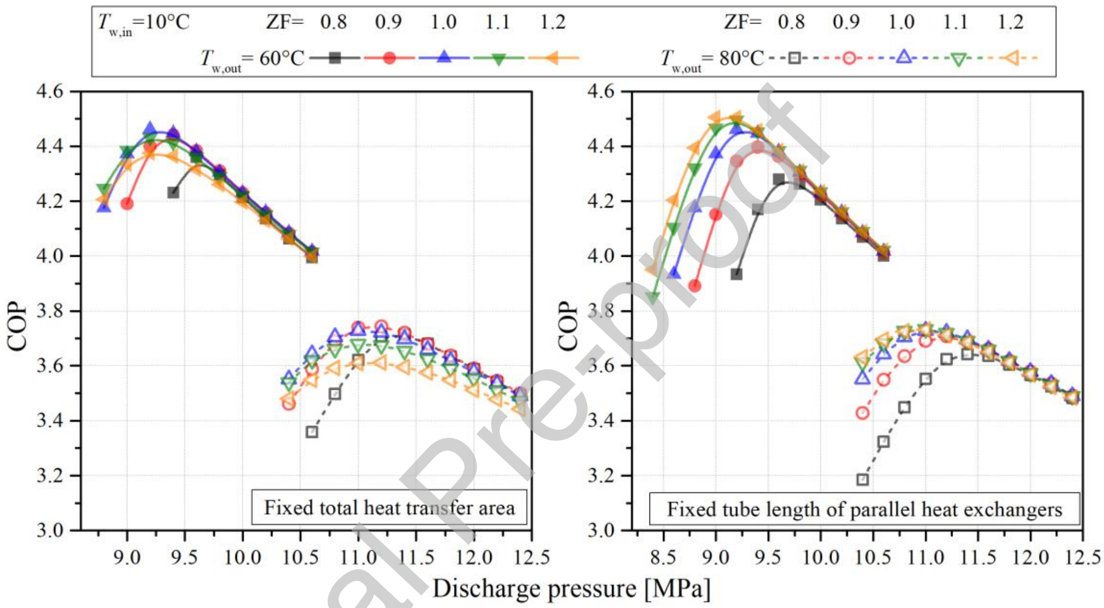

Fig. 16. COP of system with FTGC that had various zoom factors of tube diameter.

5. Conclusions

In this research, the fluted tube-in-tube gas cooler (FTGC) in the transcritical CO_2 heat pump water heater was investigated through simulation. The model validation proved that the proposed model can predict the performance of FTGC in a wide range, which can provide reference for similar applications. For comparison, the smooth tube-in-tube gas cooler (STGC) with the same geometric parameters was also simulated and discussed. The effects of different parameters on the heat transfer performance were analyzed, and the system COP under different conditions was evaluated. Several conclusions could be drawn:

(1) Generally, the heat transfer rate of the FTGC was higher than that of the STGC. With the enlarged CO_2 inlet pressure, the heat transfer rate first increased and then decreased and the maximum heat transfer rate of FTGC was 31.2% higher than that of STGC. As the CO_2 inlet temperature and CO_2 mass flow rate increased, the heat transfer rate presented a proportional increasing trend.

(2) With the increase of water inlet and outlet temperatures, the heat transfer rate decreased. When the water inlet temperature was 10℃, the heat transfer rate of FTGC was 34.47% higher than that of STGC, and this improvement reduced when the water inlet temperature increased. The position of the pinch point in the FTGC was mainly influenced by the CO_2 inlet pressure and water inlet and outlet temperatures.

(3) The benefit of the FTGC to the system COP was verified in most conditions. The maximum COP in the system with FTGC was always higher. The improvement of the maximum COP could be up to 29.41% when the water inlet temperature was 10℃ and the water outlet temperature was 80℃. However, the improvement would be impaired to 12.98% when the water inlet temperature increased to 40℃.

(4) With fixed total heat transfer area, the best maximum COP could be achieved

at the water inlet and outlet temperatures of 10℃ and 60℃ with the FTGC that had the configuration used in the experiments; when the water outlet temperature was 80℃, the decrease of parallel heat exchanger number to 2 or zoom factor of tube diameter to 0.9 could contribute to the enhancement of maximum COP.

Acknowledgement

The authors acknowledge the financial supports from the National Natural Science Foundation of China (No. 51976153), the National Science and Technology Major Project (2017-III-0010-0036) and the Foundation for Innovative Research Groups of the National Natural Science Foundation of China (No.51721004). The first author is grateful for the financial support from the China Scholarship Council and the Department of Energy and Process Engineering, Norwegian University of Science and Technology (NTNU) for his overseas study at NTNU.

References

Austin, B.T., Sumathy, K., 2011. Transcritical carbon dioxide heat pump systems: A review. Renewable and Sustainable Energy Reviews 15, 4013-4029.

Bahman, A.M., Ziviani, D., Groll, E.A., 2020. A generalized moving-boundary algorithm to predict the heat transfer rate of transcritical CO_2 gas coolers. International Journal of Refrigeration 118, 491-503.

Breidenich, C., Magraw, D., Rowley, A., Rubin, J.W., 1998. The Kyoto Protocol to the United Nations Framework Convention on Climate Change. American Journal of International Law 92, 315-331.

Chen, M., Sun, X., Christensen, R., Shi, S., Skavdahl, I., Utgikar, V., Sabharwall, P., 2016. Design and testing of helicallycoiled fluted tube heat exchangers for FHR applications, Proceedings of 11th International Topical Meeting on Nuclear Reactor Thermal Hydraulics, Operation and Safety (NUTHOS-11), pp. 9-13.

Chen, Y.-G., 2016. Pinch point analysis and design considerations of CO_2 gas cooler for heat pump water heaters. International Journal of Refrigeration 69, 136-146.

Chen, Y.-G., 2019. Optimal heat rejection pressure of CO_2 heat pump water heaters based on pinch point analysis. International Journal of Refrigeration 106, 592-603.

Dai, B., Qi, H., Dou, W., Liu, S., Zhong, D., Yang, H., Nian, V., Hao, Y., 2020a. Life cycle energy, emissions and cost evaluation of CO_2 air source heat pump system to replace traditional heating methods for residential heating in China: System configurations. Energy Conversion and Management 218, 112954.

Dai, B., Qi, H., Liu, S., Ma, M., Zhong, Z., Li, H., Song, M., Sun, Z., 2019. Evaluation of transcritical CO_2 heat pump system integrated with mechanical subcooling by utilizing energy, exergy and economic methodologies for residential heating. Energy Conversion and Management 192, 202-220.

Dai, B., Zhao, X., Liu, S., Yang, Q., Zhong, D., Hao, Y., Hao, Y., 2020b. Energetic, exergetic and exergoeconomic assessment of transcritical CO_2 reversible system combined with dedicated mechanical subcooling (DMS) for residential heating and cooling. Energy Conversion and Management 209, 112594.

Dang, C., Hihara, E., 2004. In-tube cooling heat transfer of supercritical carbon dioxide. Part 1. Experimental measurement. International Journal of Refrigeration 27, 736-747.

Ehsan, M.M., Guan, Z., Klimenko, A.Y., 2018. A comprehensive review on heat transfer and pressure drop characteristics and correlations with supercritical CO_2 under heating and cooling applications. Renewable and Sustainable Energy Reviews 92, 658-675.

Fronk, B.M., Garimella, S., 2011a. Water-coupled carbon dioxide microchannel gas cooler for heat pump water heaters: Part I - Experiments. International Journal of Refrigeration 34, 7-16.

Fronk, B.M., Garimella, S., 2011b. Water-coupled carbon dioxide microchannel gas cooler for heat pump water heaters: Part II – Model development and validation. International Journal of Refrigeration 34, 17-28.

Gnielinski, V., 1976. New equations for heat and mass transfer in turbulent pipe and channel flows. Int. Chem. Eng. 16, 359-368.

Huang, L., Aute, V., Radermacher, R., 2014. A finite volume coaxial heat exchanger model with moving boundaries and modifications to correlations for two-phase flow in fluted annuli. International Journal of Refrigeration 40, 11-23.

Lata, M., Gupta, D.K., 2020. Performance evaluation and comparative analysis of trans-critical CO_2 booster refrigeration systems with modified evaporative cooled gas cooler for supermarket application in Indian context. International Journal of Refrigeration 120, 248-259.

Lemmon, E.W., Huber, M.L., McLinden, M.O., 2013. NIST Standard Reference Database 23: Reference Fluid Thermodynamic and Transport Properties-REFPROP, Version 9.1. National Institute of Standards and Technology, Gaithersburg.

Li, J., Jia, J., Huang, L., Wang, S., 2017. Experimental and numerical study of an integrated fin and micro-channel gas cooler for a CO_2 automotive air-conditioning. Applied Thermal Engineering 116, 636-647.

Li, M., Yang, Y., Ma, Y., Wang, K., 2013. The research on gas cooler of the CO_2 trans-critical cycle. Acta Energiae Solaris Sinica 34, 1661-1666.

Liu, S.C., Li, Z., Dai, B.M., Zhong, Z.F., Li, H.L., Song, M.J., Sun, Z.L., 2019. Energetic, economic and environmental analysis of air source transcritical CO_2 heat pump system for residential heating in China. Applied Thermal Engineering 148, 1425-1439.

Lorentzen, G., Pettersen, J., 1993. A new, efficient and environmentally benign system for car air-conditioning. International Journal of Refrigeration 16, 4-12.

Minetto, S., 2011. Theoretical and experimental analysis of a CO_2 heat pump for domestic hot water. International Journal of Refrigeration 34, 742-751.

Moffat, R.J., 1988. Describing the Uncertainties in Experimental Results. Experimental Thermal and Fluid Science 1, 3-17.

Ndiaye, D., 2017. Transient model of a refrigerant-to-water helically coiled tube-in-tube heat exchanger with corrugated inner tube. Applied Thermal Engineering 112, 413-423.

Park, I.S., 2010. Numerical analysis for flow, heat and mass transfer in film flow along a vertical fluted tube. International Journal of Heat and Mass Transfer 53, 309-319.

Peng, X., Wang, D., Wang, G., Yang, Y., Xiang, S., 2020. Numerical investigation on the heating performance of a transcritical CO2 vapor-injection heat pump system.

Applied Thermal Engineering 166, 114656.

Qi, C., Li, C., Wang, G., 2017. Experimental Study on the Flow and Heat Transfer Characteristics of TiO_2-Water Nanofluids in a Spirally Fluted Tube. Nanoscale Res Lett 12, 516.

Qin, X., Zhang, D., Zhang, F., Gao, Z., Wei, X., 2020. Experimental and numerical study on heat transfer of gas cooler under the optimal discharge pressure. International Journal of Refrigeration 112, 229-239.

Rousseau, P.G., van Eldik, M., Greyvenstein, G.P., 2003. Detailed simulation of fluted tube water heating condensers. Int J Refrig 26, 232-239.

Srinivasan, V., Christensen, R.N., 1992. Experimental Investigation of Heat-Transfer and Pressure-Drop Characteristics of Flow through Spirally Fluted Tubes. Experimental Thermal and Fluid Science 5, 820-827.

Tsamos, K.M., Ge, Y.T., Santosa, I.D.M.C., Tassou, S.A., 2017. Experimental investigation of gas cooler/condenser designs and effects on a CO_2 booster system. Applied Energy 186, 470-479.

Wang, D., Shi, J.-y., Yu, B., Chen, J., 2019a. Heat Transfer Characteristics of Gas Cooler in a CO_2 Automobile Heat Pump System. 1.

Wang, L.J., Sun, D.W., Liang, P., Zhuang, L.X., Tan, Y.K., 2000. Heat transfer characteristics of carbon steel spirally fluted tube for high pressure preheaters. Energy Conversion and Management 41, 993-1005.

Wang, S., Tuo, H., Cao, F., Xing, Z., 2013. Experimental investigation on air-source transcritical CO_2 heat pump water heater system at a fixed water inlet temperature. International Journal of Refrigeration 36, 701-716.

Wang, X.W., Leong, K.C., Wong, T.N., 2017. Numerical analysis of different fluted fins for condensation on a vertical tube. Int J Therm Sci 122, 359-370.

Wang, Y., Wang, D., Yu, B., Shi, J., Chen, J., 2019b. Experimental and numerical investigation of a CO_2 heat pump system for electrical vehicle with series gas cooler configuration. International Journal of Refrigeration 100, 156-166.

Xu, X.X., Chen, G.M., Tang, L.M., Zhu, Z.J., 2011. Development and validation of helical-coil-in-fluted-tube gas cooler for CO_2 heat pump water heaters. International Journal of Energy Research 35, 1266-1273.

Yang, J., Ning, S., 2019. Experimental and Numerical Study of Double-Pipe

Evaporators Designed for CO_2 Transcritical Systems. Processes 7, 547.

Yang, Y., Li, M., Wang, K., Ma, Y., 2016. Study of multi-twisted-tube gas cooler for CO2 heat pump water heaters. Applied Thermal Engineering 102, 204-212.

Ye, Z., Wang, Y., Song, Y., Yin, X., Cao, F., 2020. Optimal discharge pressure in transcritical CO_2 heat pump water heater with internal heat exchanger based on pinch point analysis. International Journal of Refrigeration 118, 12-20.

Yu, P.-Y., Lin, K.-H., Lin, W.-K., Wang, C.-C., 2012. Performance of a tube-in-tube CO_2 gas cooler. International Journal of Refrigeration 35, 2033-2038.

Yu, Z., Tao, L., Huang, L., Wang, D., 2020. Numerical investigation on cooling heat transfer and flow characteristic of supercritical CO_2 in spirally fluted tubes. International Journal of Heat and Mass Transfer 163, 120399.

Zendehboudi, A., Ye, Z., Hafner, A., Andresen, T., Skaugen, G., 2021. Heat transfer and pressure drop of supercritical CO_2 in brazed plate heat exchangers of the tri-partite gas cooler. International Journal of Heat and Mass Transfer 178, 121641.

Zhang, F., Zhu, Y., Li, C., Jiang, P., 2018. Thermodynamic optimization of heat transfer process in thermal systems using CO_2 as the working fluid based on temperature glide matching. Energy 151, 376-386.

Zhu, D., Xu, H., Sun, Y., Qi, B., 2010. Numerical heat transfer analysis of laminar film condensation on a vertical fluted tube. Applied Thermal Engineering 30, 1159-1163.

Zhu, Y., Huang, Y., Lin, S., Li, C., Jiang, P., 2019. Study of convection heat transfer of CO_2 at supercritical pressures during cooling in fluted tube-in-tube heat exchangers. International Journal of Refrigeration 104, 161-170.

Declaration of interests

☒ The authors declare that they have no known competing financial interests or personal relationships that could have appeared to influence the work reported in this paper.

☐The authors declare the following financial interests/personal relationships which may be considered as potential competing interests: